Universal Set of Scalable Dynamically Corrected Gates for Quantum Error Correction with Always-on Qubit Couplings

Amrit De and Leonid P. Pryadko

Department of Physics and Astronomy, University of California, Riverside, California 92521, USA

(Received 24 September 2012; published 15 February 2013)

We construct a universal set of high fidelity quantum gates to be used on a sparse bipartite lattice with always-on Ising couplings. The gates are based on dynamical decoupling sequences using shaped pulses, they protect against low-frequency phase noise, and can be run in parallel on non-neighboring qubits. This makes them suitable for implementing quantum error correction with low-density parity check codes like the surface codes and their finite-rate generalizations. We illustrate the construction by simulating the quantum Zeno effect with the [[4, 2, 2]] toric code on a spin chain.

DOI: 10.1103/PhysRevLett.110.070503 PACS numbers: 03.67.Pp, 03.65.Xp, 03.67.Lx, 33.25.+k

Quantum error correction (QEC) makes it theoretically possible to perform large quantum computations with a finite per-qubit error rate [1–3]. In practice QEC is extremely difficult since the corresponding error probability threshold is small [4–9]. When only local interactions between the qubits are allowed, the estimated threshold value is the highest, around 1%, for toric and related surface codes [5,9,10]. However, as to how to implement the operations efficiently and with the required accuracy, is still an open question.

Qubits with always-on couplings are a natural model for several potential quantum computer (QC) architectures, e.g., the original Kane proposal [11], nitrogen vacancy centers in diamond [12,13], superconducting phase qubits [14,15], and circuit QED lattices [16,17]. In general, compared to their counterparts with tunable couplings, qubits with always-on couplings can be expected to have better parameter stability and longer coherence times. In addition, over sixty years of development in nuclear magnetic resonance (NMR) has yielded an amazing degree of control available to such systems [18,19]. Related techniques based on selective dynamical decoupling (DD) of parts of the system Hamiltonian, with carefully designed pulse sequences, have been further developed in application to quantum computation [20–26].

While NMR quantum computation is not easily scalable [27], it still holds several records for the number of coherently controlled qubits [19]. However, some of these have been achieved with the help of strongly modulated pulses, computer-generated single- and multi-qubit gates tailored for a particular system Hamiltonian [28–31]. While such gates can be used in other QC architectures [32], they may violate scalability.

On the other hand, NMR-inspired techniques like DD can also be used to control large systems with local interactions, where the scalability is achieved by designing pulses and sequences to a given order in the Magnus series [33] on small qubit clusters [34,35]. DD is also excellent in producing accurate control for systems where not all interactions are known as one can decouple interactions with the given symmetry [36,37]. Moreover, DD works best against errors coming from low-frequency bath degrees of freedom which tend to dominate the decoherence rates, and it does not require additional qubits. In short, DD is an excellent choice for the first level of coherence protection; its use could greatly reduce the required repetition rate of the QEC cycle.

This is well recognized in the community and applications of DD for a QC are actively investigated by a number of groups. However, most publications on the subject illustrate general principles using a single qubit as an example, leaving out the issues of design and simulation of scalable approaches to multiqubit dynamical decoupling. While the techniques for larger systems exist, they typically require longer decoupling sequences [24,36,38].

The goal of this work is to provide a scalable benchmark implementation of a universal set of accurate gates using soft pulses for a system with always-on qubit couplings. Specifically, we construct one- and two-qubit gates with built-in DD protection against low-frequency phase noise for a sparse bipartite lattice of qubits with the nearest-neighbor (NN) Ising couplings. The constructed gates use finite-amplitude shaped pulses which can be implemented experimentally. They are scalable, in the sense that the same construction works for an arbitrary lattice, and they can be executed in parallel for different qubits and/or qubit pairs. This makes them ideal for implementing QEC with quantum low-density parity check codes [39,40], in particular, the surface codes and their finite-rate generalizations [5,41,42]. In the limit of a very slow (classical) bath the gates are accurate to second order in the Magnus expansion, meaning that their infidelity scales as sixth or higher powers of the coupling, in units of inverse pulse duration. We demonstrate the accuracy of the constructed gates by simulating the quantum Zeno effect [43,44] for the [[4, 2, 2]] error-detecting toric code, in repeated cycles, on an Ising chain. The simulations are done with five qubits, using classical correlated noise as a source of dephasing.

Two techniques are essential to our work. First, the use of NMR-style self-refocusing pulses [34,45–47], which (to a given order) work as drop-in replacements for hard, δ-function-like pulses. In our simulations, we use the second-order pulses designed and characterized in Refs. [34,35,46,48]. The second technique is the Eulerian path construction [23], and its extension, the dynamically corrected gates [38,49,50], which allow for the construction of composite pulses accurate to a given order of the Magnus expansion.

We construct our gates for a collection of qubits arranged on an arbitrary sparse bipartite graph $\mathcal{G}$, with the edge set $\mathcal{E}$, with an Ising coupling for every edge,

$$H_S \equiv \frac{1}{2}\sum_{(ij)\in\mathcal{E}} J_{ij}\sigma_i^z\sigma_j^z, \tag{1}$$

arbitrary (within the bandwidth) single-qubit control,

$$H_C \equiv \frac{1}{2}\sum_i \sum_{\mu=x,y,z} \sigma_i^\mu V_{i\mu}(t), \tag{2}$$

in the presence of low-frequency phase noise

$$H_N \equiv \frac{1}{2}\sum_i \sigma_i^z B_i + H_B. \tag{3}$$

Here, B_i are the bath coupling operators (e.g., from low-frequency phonons or nuclear spins), and H_B is the corresponding bath Hamiltonian independent from σ_i^μ.

Decoherence resulting from higher-frequency bath modes, e.g., as described by the Lindblad equation [51], can also be introduced, but at later design stages, since DD is not effective against such decoherence. While we do not consider Markovian decoherence here, we mention in passing that the main effects of DD are the suppression of equilibrium population asymmetries (qubits are constantly flipped), and with soft-pulse DD, the redistribution of decoherence rates between the channels [48]. For example, even if dephasing is dominant for nondriven qubits, any sequence of finite-width pulses creates some longitudinal relaxation (compensated by a reduction of the dephasing rate).

To construct the CNOT gate, we use the identity [52]

$$\mathrm{CNOT}_{cd} = e^{i\pi/4} Y_c \bar{X}_c \bar{Y}_c X_d \bar{Y}_d e^{-i\pi/4\sigma_c^z\sigma_d^z} Y_d, \tag{4}$$

where $X_i \equiv \exp(-i\frac{\pi}{4}\sigma_i^x)$, $Y_i \equiv \exp(-i\frac{\pi}{4}\sigma_i^y)$, are $\pi/2$ unitaries, and $\bar{X}_i$, $\bar{Y}_i$ denote the corresponding conjugate gates [in simulations we use the equivalent form with $Y_c\bar{X}_c\bar{Y}_c \equiv Z_c$].

To implement the two-qubit zz-rotation gate, $e^{-i\pi/4\sigma_c^z\sigma_d^z}$, we run two period-$16\tau_p$ decoupling sequences on the sublattices A and B, $V_A(t)$ and $V_B(t)$ in Fig. 1, where each pulse of duration τ_p is a symmetric π pulse applied in the x direction. When the pulses are second-order self-refocusing pulses (e.g., $Q_1(\pi)$ from Refs. [34,46] shown), these sequences suppress the effect of the Ising couplings H_S and the noise H_N to second order in the Magnus expansion, meaning that the effective Hamiltonian is just H_B, with the error scaling as $\propto \tau_p^2$. This gives the error in the unitary matrix scaling as $\propto \tau_p^3$, and the corresponding infidelity $1\text{-}F$ scaling as $\propto \tau_p^6$ (we use the average fidelity F expressed in terms of the unitary evolution matrix, see Appendix of Ref. [46]).

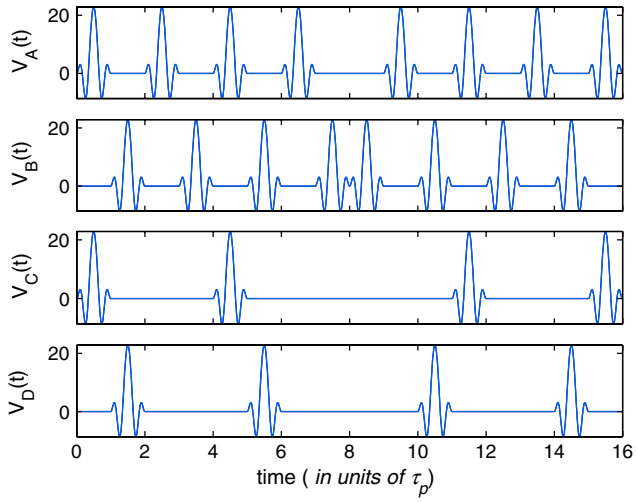

FIG. 1 (color online). Pulse sequences used to implement two-qubit zz rotations on a bipartite lattice with Ising couplings. Global sequences of π pulses in the x direction, $V_A(t)$ and $V_B(t)$, are executed on the idle qubits of the two sublattices. These decouple the interqubit Ising couplings and also the single-qubit low-frequency phase noise terms. In order to couple two neighboring qubits, the sequences V_A, V_B are respectively replaced by V_C, V_D on these qubits. This produces an effective Ising Hamiltonian with half of the original coupling. Shown are $Q_1(\pi)$ second-order self-refocusing pulse shapes [34,46] used in the simulations.

To turn on the coupling between two neighboring qubits c, d, the two sublattice sequences on these qubits are replaced with $V_C(t)$ and $V_D(t)$, respectively, see Fig. 1. These sequences are chosen so that the Ising coupling between these qubits is only removed half of the time, while the coupling to other qubits continues to be removed. More precisely, with second-order pulses, the effective Hamiltonian is $H_B + (J/4)\sigma_c^z\sigma_d^z + \mathcal{O}(\tau_p^2)$. Repeating this sequence m times gives the system evolution

$$U_{zz} = \exp(-i\alpha\sigma_c^z\sigma_d^z), \qquad \alpha = 4mJ\tau_p, \tag{5}$$

with the error scaling as $\propto m\tau_p^3$, where the term associated with the bath evolution is suppressed. Such sequences can be run simultaneously on many pairs of qubits as long as qubits from different pairs are not mutually coupled.

We implement single-qubit rotations with the leading-order dynamically corrected gates (DCGs) [38,49], using the pulse sequences in Fig. 2. Again, two decoupling sequences, $V_1(t)$ and $V_2(t)$, are run globally on the two sublattices; additional pulses are inserted for the qubits to be rotated [$V_3(t)$ in Fig. 2 shows an implementation of the $\pi/2$ rotation with respect to Y axis on a sublattice-A qubit]. The Hadamard gates are implemented using these single qubit rotations and the identity $U_H = e^{-i\pi/2}\exp(i\frac{\pi}{4}\sigma_y)\exp(i\frac{\pi}{2}\sigma_x)$.

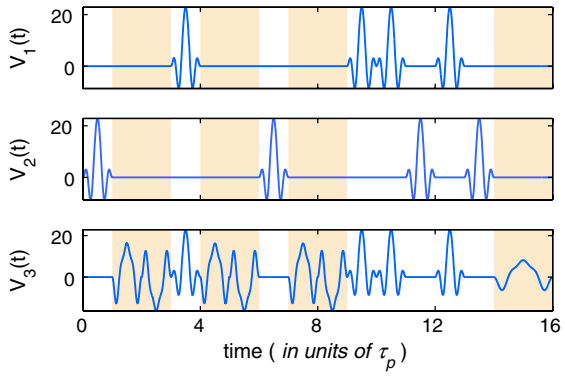

FIG. 2 (color online). Pulse sequence used to implement single-qubit rotations. The sequences of π pulses in the x direction, $V_1(t)$ and $V_2(t)$, are executed globally on idle qubits of the two sublattices. A single-qubit rotation is implemented as a DCG by adding three pulse-antipulse combinations and the stretched pulse in the shaded regions (y axis). The sequence $V_3(t)$, where pulses in the shaded regions are $Q_1(\pi/2)$, corresponds to a $(\pi/2)_Y$ operation on a sublattice-A qubit. Such gates can be executed on any set of non-neighboring qubits.

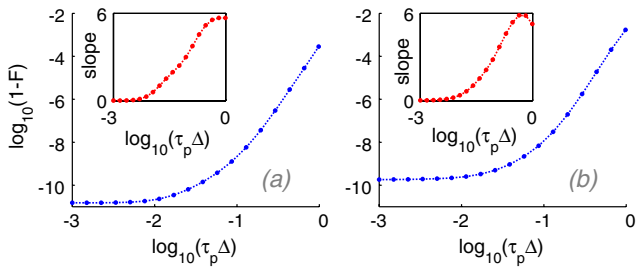

FIG. 3 (color online). (a) The infidelity of the gate in Fig. 2 and (b) the infidelity of the complete CNOT gate between qubits 2 and 3 of a four-qubit NN Ising chain as a function of rms chemical shift Δ (pulse sequences not shown). For small Δ the errors saturate because of the fixed J; when Δ is large, chemical shifts dominate the errors. The insets show the corresponding slopes; the slope of ~ 6 [infidelity $\propto (\tau_p\Delta)^6$] indicates that the on-site chemical shifts are decoupled to quadratic order. Analogous calculations with first-order pulses [34,46] $S_1(\pi)$ and $S_1(\pi/2)$ give first-order [infidelity $\propto (\tau_p\Delta)^4$] decoupling and 2 orders of magnitude higher infidelities (not shown); Gaussian pulses increase infidelities by up to 5 orders of magnitude.

Nominally, DCGs guarantee first-order decoupling with any pulse shape. However, in our case, the decoupling sequences $V_i(t)$, $i = 1, 2$, do not go over the complete single-qubit groups. Thus, unoptimized (e.g., Gaussian) pulses can produce unitary errors scaling linearly with the pulse duration τ_p; one needs first-order self-refocusing pulses [34,45,46] to get first-order decoupling. In the case of the second-order pulses (e.g., $Q_1(\phi)$ [46]), the remaining order-τ_p^2 errors are all proportional to different commutators $[B_i, B_j]$ and $[H_B, B_i]$, which gives second-order decoupling (infidelity $\propto \tau_p^6$) when the operators B_i are replaced by c numbers Δ_i (cf. chemical shifts in NMR).

These predictions are confirmed in Fig. 3 which shows the average infidelities for a single $(\pi/2)_Y$ rotation of qubit 3 [Fig. 3(a)] and a complete CNOT_{23} gate [Fig. 3(b)] as a function of the rms chemical shift Δ (in units of τ_p^{-1}), obtained numerically for a four-qubit Ising chain. The simulations are done with a custom C++ program using fourth-order Runge-Kutta algorithm for integrating the unitary dynamics and the Eigen3 library [53] for matrix arithmetics. We fix the value of $J_{ij} = J = \pi/(16m\tau_p)$ with $m = 5$ repetitions of the basic sequence [see Eqs. (4) and (5) and Fig. 1] in the CNOT gate; with the addition of four single-qubit DCGs [see Fig. 2] the CNOT duration is $t_{\text{CNOT}} = 9 \times 16\tau_p = 144\tau_p$. For small Δ, the infidelities are dominated by the decoupling accuracy of the interqubit interactions, while they scale as $\propto \Delta^6\tau_p^6$ for large Δ, see the graphs of the corresponding slopes in the insets.

We illustrate the performance of the designed gates by simulating the quantum Zeno effect [43,44] using the four-qubit toric error-detecting code [10,54]. We used zero-mean classical stationary Gaussian stochastic processes with Gaussian correlations, $\langle B_i(t)B_j(t')\rangle = \sigma^2\delta_{ij}e^{-(t-t')^2/\tau_c^2}$, as the source of decoherence. These are obtained by applying the Gaussian filter to discrete sets of uncorrelated random numbers drawn from the Gaussian distribution, and using the standard cubic spline interpolation with the result.

The [[4, 2, 2]] toric code is a stabilizer code [55,56] encoding an arbitrary state of $k = 2$ qubits into a 2^2-dimensional subspace $\mathcal{Q}$ of the 4-qubit Hilbert space. The subspace $\mathcal{Q}$ is the common $+1$ eigenspace of the two stabilizer generators, $G_x = \sigma_1^x\sigma_2^x\sigma_3^x\sigma_4^x$ and $G_z = \sigma_1^z\sigma_2^z\sigma_3^z\sigma_4^z$. We use the following explicit map (up to normalization) for the logical qubits

$$|\tilde{0}\tilde{0}\rangle = |0000\rangle + |1111\rangle, \quad |\tilde{0}\tilde{1}\rangle = |0011\rangle + |1100\rangle,$$
$$|\tilde{1}\tilde{0}\rangle = |0101\rangle + |1010\rangle, \quad |\tilde{1}\tilde{1}\rangle = |0110\rangle + |1001\rangle. \tag{6}$$

An application of any single-qubit error, i.e., a Pauli operator σ_i^μ, $\mu = x, y, z$, takes the encoded wave function to one of the three orthogonal subspaces, where one or both of the eigenvalues of G_x, G_z (these eigenvalues form the error syndrome) equal -1. The code has distance $d = 2$ since some two-qubit errors, e.g., $\sigma_1^z\sigma_2^z$, act within the code space and cannot be detected.

In the presence of the error Hamiltonian (3), to leading order in the perturbation, the original wave function ψ_0 evolves into a superposition of orthogonal terms $A_0|\psi_0\rangle + A_i^\mu\sigma_i^\mu|\psi_0\rangle$. In general, the coefficients A_0, A_i are operators acting on the bath degrees of freedom and the state's fidelity is given by $F \equiv \text{Tr}_B(A_0^\dagger A_0\rho_B)$, where the trace is taken over the bath degrees of freedom with the density matrix ρ_B. With the same accuracy, F is also the probability that the measurement returns $G_x = G_z = 1$. For weak perturbation, and for times, t, that are small compared to the bath correlation time τ_c, the infidelity $1 - F$ scales quadratically with t. Thus frequent projective measurements of the generators ensure preservation of the wave function with high probability—the quantum Zeno effect [43,44]. At higher orders, there will be errors spanning

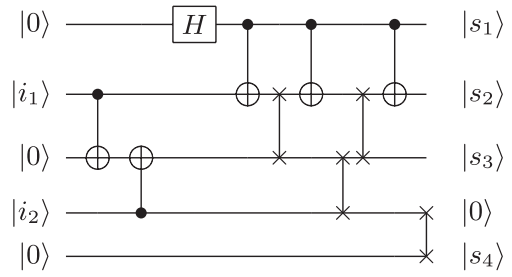

FIG. 4. Encoding circuit for the [[4, 2, 2]] code implemented on a spin chain using four exchange gates (each implemented with three CNOTS), five CNOT gates, and a Hadamard gate H. Input qubits i_1, i_2 can be in an arbitrary two-qubit state, on the output the circuit returns an equivalent linear combination of the states in the code, see Eq. (6), using qubits s_j, $j = 1, \ldots, 4$, and an ancilla initialized for the stabilizer measurement circuit in Fig. 5. The decoding is done by reversing this circuit.

multiple qubits which may decrease the fidelity even when the circuit is formally successful (i.e., measurements yield $G_x = G_z = 1$, see Figs. 6 and 7).

Using the constructed DD gates, we simulated the decoding and encoding and ancilla-based stabilizer measurement circuits (Figs. 4 and 5), where we use standard quantum circuit notations [56,57]. A projective single-qubit measurement is implemented simply as an instantaneous projection to the $|0\rangle$ state of the ancilla.

Samples of the simulation results are shown in Figs. 6 and 7 with the time axis starting at the end of the encoding (see Fig. 4). They show the time-dependence of average infidelities (which assume that each syndrome measurement returns the original "correct" value, $G_x = G_z = 1$; only such results are preserved), and the accumulated circuit success probability (fraction of preserved data sets). These results are averaged over 20 instances of classical correlated noise and with the syndrome measurements alternating between G_x and G_z.

It is clear that the dynamical decoupling and the Zeno effect are both contributing to improving the fidelity, and both get better with decreasing noise. This indicates that the errors contributing to the infidelity of the constructed gates are not dominated by high-weight errors which would be undetectable by the code [58].

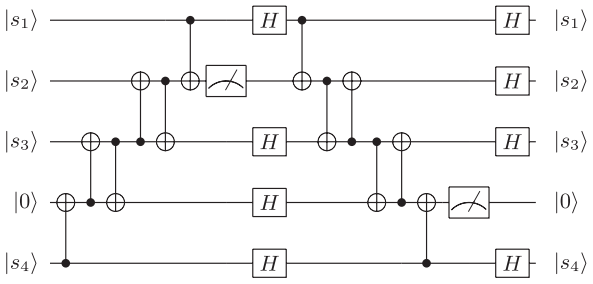

FIG. 5. Measurement circuit for the [[4, 2, 2]] code on a spin chain with a shuttling ancilla. The ancilla is first shuttled up for the G_z measurement and then shuttled down for the G_x measurement. The entire circuit is repeated for every Zeno cycle.

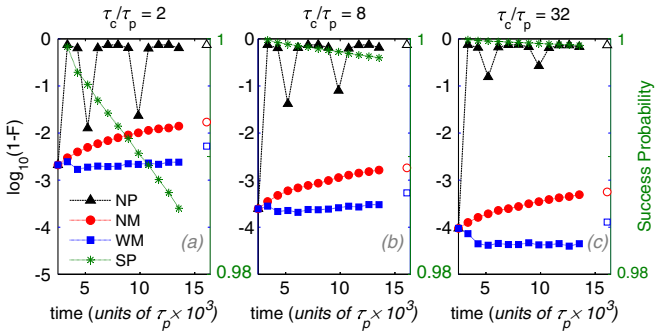

FIG. 6 (color online). Infidelities during the Zeno cycle for different noise correlation times but with the same noise amplitude $\sigma = 10^{-3}/\tau_p$. The different curves correspond to cases where no pulses are applied (NP), DD pulses are applied but no measurements are made (NM), and with the syndrome measurements (WM). Closed and open symbols respectively represent the infidelities during the syndrome measurements and at the end of the final decoding. Note that the axis for the cumulative success probability (SP) is on the right.

The infidelity sharply increases with shorter noise correlation times; this results from the asymmetry of the DCGs, see Fig. 2. We have also constructed [58] symmetrized DCGs which give second-order decoupling for arbitrary bath operators B_i when used with the pulses constructed in Ref. [47]; we expect such gates to have a much better accuracy for smaller noise correlation time, down to the gate duration, $\tau_c \geq 32\tau_p$.

In conclusion, we implemented a universal set of one- and two-qubit gates for a system with always-on qubit coupling. The gates are based on DD techniques and have an added benefit of protection against low-frequency phase noise.

One application of these constructed gates is for implementing toric codes on a square lattice, where one sublattice would be used for actual qubits, and the other sublattice for ancillas. This way, measurement of the entire syndrome can be done in just two cycles, each of four CNOTS in duration, plus some single-qubit gates. The same sequences would also work for an arbitrary quantum low-density parity check code, if the couplings between the qubits and the ancillas form the corresponding Tanner graph [59]. In particular, for

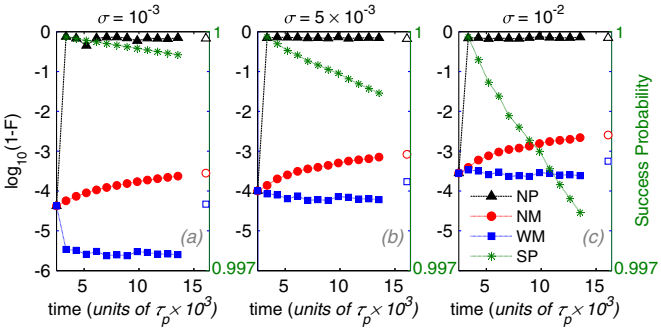

FIG. 7 (color online). Same as Fig. 6 but with fixed noise correlation time $\tau_c = 128\tau_p$ with the rms noise amplitudes σ as indicated.

hypergraph-product and related codes [41,42] one can use the square lattice layout with additional connections [60].

We wish to thank K. Khodjasteh, D. Lidar, and L. Viola for a number of useful discussions. This work was supported in part by the U.S. Army Research Office under Grant No. W911NF-11-1-0027, and by the NSF under Grant No. 1018935.

[1] P. W. Shor, Phys. Rev. A **52**, R2493 (1995).
[2] E. Knill and R. Laflamme, Phys. Rev. A **55**, 900 (1997).
[3] C. H. Bennett, D. P. DiVincenzo, J. A. Smolin, and W. K. Wootters, Phys. Rev. A **54**, 3824 (1996).
[4] E. Knill, R. Laflamme, and W. H. Zurek, Science **279**, 342 (1998).
[5] E. Dennis, A. Kitaev, A. Landahl, and J. Preskill, J. Math. Phys. (N.Y.) **43**, 4452 (2002).
[6] A. M. Steane, Phys. Rev. A **68**, 042322 (2003).
[7] A. G. Fowler, C. D. Hill, and L. C. L. Hollenberg, Phys. Rev. A **69**, 042314 (2004).
[8] A. G. Fowler, S. J. Devitt, and L. C. L. Hollenberg, Quantum Inf. Comput. **4**, 237 (2004).
[9] R. Raussendorf and J. Harrington, Phys. Rev. Lett. **98**, 190504 (2007).
[10] A. Y. Kitaev, Ann. Phys. (Amsterdam) **303**, 2 (2003).
[11] B. E. Kane, Nature (London) **393**, 133 (1998).
[12] G. J. Milburn, Science **330**, 1188 (2010).
[13] G. de Lange, D. Ristè, V. V. Dobrovitski, and R. Hanson, Phys. Rev. Lett. **106**, 080802 (2011).
[14] R. McDermott, R. W. Simmonds, M. Steffen, K. B. Cooper, K. Cicak, K. D. Osborn, S. Oh, D. P. Pappas, and J. M. Martinis, Science **307**, 1299 (2005).
[15] J. M. Martinis, Quantum Inf. Process. **8**, 81 (2009).
[16] D. I. Schuster, A. A. Houck, J. A. Schreier, A. Wallraff, J. M. Gambetta, A. Blais, L. Frunzio, J. Majer, B. Johnson, M. H. Devoret, S. M. Girvin, and R. J. Schoelkopf, Nature (London) **445**, 515 (2007).
[17] J. Majer, J. M. Chow, J. M. Gambetta, J. Koch, B. R. Johnson, J. A. Schreier, L. Frunzio, D. I. Schuster, A. A. Houck, A. Wallraff, A. Blais, M. H. Devoret, S. M. Girvin, and R. J. Schoelkopf, Nature (London) **449**, 443 (2007).
[18] L. M. K. Vandersypen and I. L. Chuang, Rev. Mod. Phys. **76**, 1037 (2005).
[19] B. Criger, G. Passante, D. Park, and R. Laflamme, Phil. Trans. R. Soc. A **370**, 4620 (2012).
[20] L. Viola, S. Lloyd, and E. Knill, Phys. Rev. Lett. **83**, 4888 (1999).
[21] J. A. Jones and E. Knill, J. Magn. Reson. **141**, 322 (1999).
[22] L. Viola, Phys. Rev. A **66**, 012307 (2002).
[23] L. Viola and E. Knill, Phys. Rev. Lett. **90**, 037901 (2003).
[24] K. Khodjasteh and D. A. Lidar, Phys. Rev. Lett. **95**, 180501 (2005).
[25] G. S. Uhrig, Phys. Rev. Lett. **98**, 100504 (2007).
[26] A. M. Souza, G. A. Álvarez, and D. Suter, Phys. Rev. Lett. **106**, 240501 (2011).
[27] J. A. Jones, Prog. Nucl. Magn. Reson. Spectrosc. **38**, 328 (2001).
[28] E. M. Fortunato, M. A. Pravia, N. Boulant, G. Teklemariam, T. F. Havel, and D. G. Cory, J. Chem. Phys. **116**, 7599 (2002).
[29] M. D. Price, S. S. Somaroo, A. E. Dunlop, T. F. Havel, and D. G. Cory, Phys. Rev. A **60**, 2777 (1999).
[30] M. D. Price, S. S. Somaroo, C. H. Tseng, J. C. Gore, A. H. Fahmy, T. F. Havel, and D. G. Cory, J. Magn. Reson. **140**, 371 (1999).
[31] M. D. Price, T. F. Havel, and D. G. Cory, New J. Phys. **2**, 10 (2000).
[32] J. J. Vartiainen, A. O. Niskanen, M. Nakahara, and M. M. Salomaa, Phys. Rev. A **70**, 012319 (2004).
[33] C. P. Slichter, *Principles of Magnetic Resonance* (Springer-Verlag, New York, 1992), 3rd ed.
[34] P. Sengupta and L. P. Pryadko, Phys. Rev. Lett. **95**, 037202 (2005).
[35] L. P. Pryadko and P. Sengupta, Phys. Rev. B **73**, 085321 (2006).
[36] M. Stollsteimer and G. Mahler, Phys. Rev. A **64**, 052301 (2001).
[37] Y. Tomita, J. T. Merrill, and K. R. Brown, New J. Phys. **12**, 015002 (2010).
[38] K. Khodjasteh and L. Viola, Phys. Rev. Lett. **102**, 080501 (2009).
[39] M. S. Postol, arXiv:quant-ph/0108131v1.
[40] D. J. C. MacKay, G. Mitchison, and P. L. McFadden, IEEE Trans. Inf. Theory **50**, 2315 (2004).
[41] J.-P. Tillich and G. Zemor, in *IEEE International Symposium on Information Theory, ISIT 2009.* (IEEE, New York, 2009), pp. 799–803.
[42] A. A. Kovalev and L. P. Pryadko, *IEEE International Symposium on Information Theory Proceedings (ISIT)* (IEEE, New York, 2012), pp. 348–352.
[43] P. Facchi and S. Pascazio, Phys. Rev. Lett. **89**, 080401 (2002).
[44] P. Facchi, S. Pascazio, A. Scardicchio, and L. S. Schulman, Phys. Rev. A **65**, 012108 (2001).
[45] W. S. Warren, J. Chem. Phys. **81**, 5437 (1984).
[46] L. P. Pryadko and P. Sengupta, Phys. Rev. A **78**, 032336 (2008).
[47] S. Pasini, T. Fischer, P. Karbach, and G. S. Uhrig, Phys. Rev. A **77**, 032315 (2008).
[48] L. P. Pryadko and G. Quiroz, Phys. Rev. A **77**, 012330 (2008).
[49] K. Khodjasteh and L. Viola, Phys. Rev. A **80**, 032314 (2009).
[50] K. Khodjasteh, D. A. Lidar, and L. Viola, Phys. Rev. Lett. **104**, 090501 (2010).
[51] G. Lindblad, Commun. Math. Phys. **48**, 119 (1976).
[52] A. Galiautdinov and M. Geller, arXiv:quant-ph/0703208v1.
[53] G. Guennebaud, B. Jacob *et al.*, Eigen v3, http://eigen.tuxfamily.org (2010).
[54] M. Grassl, T. Beth, and T. Pellizzari, Phys. Rev. A **56**, 33 (1997).
[55] D. Gottesman, Ph.D. thesis, Caltech, 1997.
[56] M. A. Nielsen and I. L. Chuang, *Quantum Computation and Quantum Infomation* (Cambridge University Press, Cambridge, England, 2000).
[57] A. Barenco, C. H. Bennett, R. Cleve, D. P. DiVincenzo, N. Margolus, P. Shor, T. Sleator, J. A. Smolin, and H. Weinfurter, Phys. Rev. A **52**, 3457 (1995).
[58] A. De and L. P. Pryadko (unpublished).
[59] R. Tanner, IEEE Trans. Inf. Theory **27**, 533 (1981).
[60] A. A. Kovalev and L. P. Pryadko, arXiv:1208.2317 [Phys. Rev. A (to be published)].